Theoretical Investigation on the Mechanism and Thermal Rate Constants for the Reaction of Atomic O (^{3}P) with CHF_2Cl

Qingzhu Zhang, Yueshu Gu,* and Shaokun Wang

School of Chemistry and Chemical Engineering, Shandong University, Jinan 250100, P. R. China

Received: May 21, 2002; In Final Form: January 31, 2003

The hydrogen abstraction reaction of atomic O (^{3}P) with CHF_2Cl has been studied theoretically for the first time using ab initio molecular orbital theory. Two nearly degenerate saddle points of ^{3}A″ and ^{3}A′ symmetries have been located for this hydrogen abstraction reaction from the C−H bond. The potential energy surface information has been obtained at the MP2 level with the 6-311G(2d,p) basis set. Energies along the minimum energy path have been improved by a series of single-point ab initio QCISD(T)//MP2 calculation. Changes of geometries, generalized normal-mode vibrational frequencies, and potential energies along the reaction path are discussed. The kinetics nature is obtained using canonical variational transition state theory (CVT) with the small-curvature tunneling (SCT) correction method over a wide temperature range of 200∼3000 K. The result shows that the variational effect is small, and in the lower-temperature range, the SCT effect is important for the title reaction. The calculated CVT/SCT rate constants exhibit typical non-Arrhenius behavior, and a three-parameter rate-temperature formula is fitted as follows (in units of cm^3 molecule^{-1} s^{-1}): $k(T) = 4.75 \times 10^{-18} T^{2.26} \exp(-4318.02/T)$. The calculated rate constants are compared with the available experimental values.

1. Introduction

The importance of haloalkanes in atmospheric chemistry is well-established.[1−3] Chlorofluorocarbons (CFCs) are known to be responsible for the depletion of the ozone layer in the stratosphere and greenhouse effects.[4−5] With low global environmental impact, hydrofluorocarbons (HFCs) and hydrochlorofluorocarbons (HCFCs) have been proposed as potential replacements for chlorofluorocarbons (CFCs).[6−7] The reactions of HFCs and HCFCs with various radicals such as H, O (^{3}P, ^{1}D), OH, and Cl have been the active subject of many studies for a long time.[8−12] The relevant kinetics data are desirable not only to determine the fates of HFCs and HCFCs in the stratosphere but also to understand the mechanism of fire suppression.

In this paper, we report a theoretical study on the reaction of CHF_2Cl with O (^{3}P). The reasons for initiating such a work are 2-fold. First, the reaction proceeds via a direct hydrogen abstraction mechanism, which is different apparently from the insertion mechanism for the reaction of CHF_2Cl with O (^{1}D).[13] Second, the theoretical study on this hydrogen abstraction reaction is particularly challenging because the approach of the O (^{3}P) to CHF_2Cl with C_s symmetry proceeds over two potential energy surfaces (PESs), ^{3}A′+ ^{3}A″, generated by the pseudo-Jahn−Teller effect. Indeed, for C_s symmetry, the irreducible representation is ^{3}A′+ ^{3}A″(2) for reactants and ^{3}A′+ ^{3}A″+ ^{1}A′+ ^{1}A″ for products, and therefore, both asymptotes adiabatically correlate through the PESs ^{3}A′and ^{3}A″ in C_s. However, despite its experimental and theoretical importance, the kinetics work about this reaction was very limited. Only two experimental reports are on record.[14,15] To our best knowledge, little theoretical attention has been paid to this reaction.

In this paper, we have first calculated geometrical parameters, frequencies, and energies of the reactant, saddle points, and products for this hydrogen abstraction reaction from CHF_2Cl by O (^{3}P). In a second step, we have carried out the kinetics calculation. Several important features of this study are the following: (1) The reaction mechanism has been revealed at high levels of ab initio molecule orbital theory. (2) The energy profile surface has been obtained at the QCISD(T)/6-311+G-(3df,2p)//MP2/6-311G(2d,p) level. (3) The kinetics nature has been studied in the temperature range from 200 to 3000 K using interpolated canonical variational transition-state theory (CVT)[16−18] and the centrifugal-dominant, small-curvature tunneling approximation (SCT),[19] including information at the reactants, products, saddle point, and extra points along the minimum energy path. (4) The non-Arrhenius expression has been fitted. (5) The calculated rate constants are compared with the limited experimental values.

2. Computation Methods

Ab initio calculations have been carried out using Gaussian 94 programs.[20] In the whole paper, MP2 (second-order perturbation Moller−Plesset method)[21] and QCISD(T) (a Quadratic CI calculation including single and double substitutions with a triples contribution to the energy added)[22] denote the unrestricted versions, UMP2 and UQCISD(T). The geometries of the reactant, saddle points, and products have been optimized at the MP2/6-311G(2d,p) level. The vibrational frequencies have been calculated at the same level of theory in order to determine the nature of the stationary points, the zero-point energy (ZPE), and the thermal contributions to the free energy of activation. An intrinsic reaction coordinate (IRC) calculation confirmed that the saddle point connects the designated reactants and products. At the MP2/6-311G(2d,p) level, the minimum energy paths (MEP) were constructed for both ^{3}A′ and ^{3}A″ surfaces independently, starting from the respective saddle point geometries and going downhill to both the asymptotic reactant and product channel with a gradient step size of 0.02 amu$^{1/2}$ bohr.

* To whom correspondence should be addressed. E-mail: guojz@icm.sdu.edu.cn. Fax: 0531-8564464.

10.1021/jp021256p CCC: $25.00
Published on Web 04/03/2003

TABLE 1: Calculated Vibrational Frequencies (in cm^{-1}) and the Zero-Point Energies (in kcal/mol) for the Reactant, Products, and Saddle Points Involved in the Reaction of O (^3P) with CHF_2Cl at the MP2/6-311G(2d,p) Level[a]

species	frequencies									ZPE
CHF_2Cl	3196(a′)	1410(a″)	1362(a′)	1168(a′)	1137(a″)					14.97
	813(a′)	600(a′)	414(a′)	370(a″)						
	3025	*1345*	*1312*	*1178*	*1116*	*808*	*596*	*421*	*369*	
CF_2Cl	1252(a″)	1182(a′)	778(a′)	608(a′)	425(a′)					6.60
	370(a″)									
	1208	*1148*	*761*	*599*						
OH	3776									5.40
	3735									
TS(^{3}A″)	1214(a″)	1188(a′)	1106(a′)	961(a″)	917(a′)					10.62
	639(a′)	442(a′)	376(a′)	370(a″)	122(a″)					
	93(a′)	2663i(a′)								
TS(^{3}A′)	1251(a′)	1223(a″)	1177(a′)	1045(a″)	892(a′)					10.93
	650(a′)	440(a′)	392(a′)	370(a″)	103(a″)					
	100(a′)	2674i(a′)								

[a] The values in italics are the experimental data.[25−26]

Along these MEPs, the reaction coordinate, *s*, is defined as the signed distance from the saddle point, with $s > 0$ referring to the product side. At some points along the MEP, the matrix of force constants was computed in order to do the following calculations of the canonical variational rate constants.

Although the geometrical parameters and the frequencies of various species can be determined satisfactorily at the MP2/6-311G(2d,p) level, the energies obtained at this level may not be accurate enough for the subsequent kinetics calculation. Therefore, a higher level, QCISD(T), and a more flexible basis set, 6-311+G(3df,2p), were employed to calculate the energies of various species.

The initial information obtained from our ab initio calculations allowed us to calculate the variational transition state rate constant including an estimation of the tunneling effect contribution to reactivity. The canonical variational theory (CVT) rate constant for temperature *T* is given[16−18]

$$k^{\mathrm{CVT}}(T) = \min_{s} k^{\mathrm{GT}}(T, s) \tag{1}$$

where

$$k^{\mathrm{GT}}(T,s) = \frac{\sigma k_{\mathrm{B}} T}{h} \frac{Q^{\mathrm{GT}}(T,s)}{\Phi^{\mathrm{R}}(T)} e^{-V_{\mathrm{MEP}}(s)/k_{\mathrm{B}}T} \tag{2}$$

where, $k^{\mathrm{GT}}(T, s)$ is the generalized transition state theory rate constant at the dividing surface *s*, σ is the symmetry factor (the number of equivalent reaction-paths, which were assumed to be 1 and 2 for the forward and reverse reactions, respectively), k_{B} is Boltzmann's constant, *h* is Planck's constant, $\Phi^{\mathrm{R}}(T)$ is the reactant partition function per unit volume, excluding symmetry numbers for rotation, and $Q^{\mathrm{GT}}(T, s)$ is the partition function of a generalized transition state at *s* with a local zero of energy at $V_{\mathrm{MEP}}(s)$ and with all rotational symmetry numbers set to unity. The kinetics calculation has been carried out using the POLYRATE 7.8 program.[23] The IVTST-M method was chosen. The rotational partition functions were calculated classically, and the vibrational modes were treated as quantum-mechanical separable harmonic oscillators. Only the centrifugal-dominant small-curvature tunneling effect correction method was used in our calculation of the rate constant. Methods for the large-curvature cases have been developed,[24] but they require more information about the PES than was determined in the present study. Finally, the total rate constants are obtained as the sum of the calculated rate constants for the ^{3}A′ and ^{3}A″ surfaces.

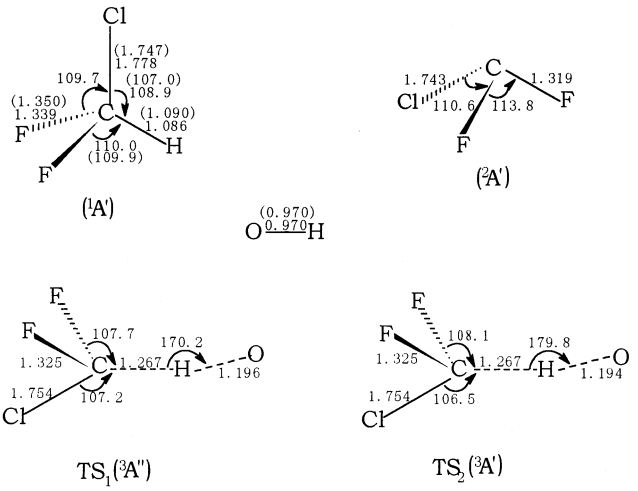

Figure 1. MP2/6-311G(2d,p) optimized geometries for the stationary points. Distances are in angstroms, and angles are in degrees. The values in parentheses are experimental data.[25]

3. Result and Discussion

The optimized geometries of the reactant, saddle points, and products are shown in Figure 1. The vibrational frequencies of the reactant, products, and saddle points are listed in Table 1. The potential barrier ΔE and the reaction enthalpy ΔH calculated are summarized in Table 2. The C−H bond dissociation energy in CHF_2Cl is also depicted in Table 2. Figure 2 depicts energy profile for the ^{3}A′ and ^{3}A″ potential energy curves with respect to their minima at the MP2/6-311G(2d,p) level. Figure 3 shows the classical potential energy (V_{MEP}) and vibrationally adiabatic potential energy (V_a^G) curves as a function of distance along the reaction coordinate *s* at the QCISD(T)/6-311+G(3df,2p)//MP2/6-311G(2d,p) level on the ^{3}A″ surface. Change curves of generalized normal-mode vibrational frequencies with the reaction coordinate *s* for the ^{3}A″ surface are shown in Figure 4. Figure 5 shows the total reaction path curvature as functions of *s* at the MP2 level. The calculated TST, CVT, and CVT/SCT rate constants along with the experimental values are presented in Table 3 and Figures 6 and 7 over the temperature ranges of 200∼3000 K and 350∼1000 K, respectively.

3.1. Reaction Mechanism. *a. Geometry and Frequency.* In the MP2/6-311G(2d,p) optimization, the values of $\langle S^2 \rangle$ are always in the range of 0.750∼0.758 for doublets and in the range of 2.000∼2.046 for triplets. After spin annihilation, the values of $\langle S^2 \rangle$ are 0.750 for doublets and 2.000 for triplets, where 0.750 and 2.000 are the exact values for a pure doublet and for

TABLE 2: Calculated Potential Barrier ΔE and Reaction Enthalpy ΔH and C−H Bond Dissociation Energies at 0 K Using the MP2/6-311G(2d,p) Optimized Geometries and ZPE Corrections[a]

	ΔE			
levels	3A″	^{3}A′	ΔH	D_0(C−H)
MP2/6-311G(2d,p)	16.57 (20.92)	16.83 (20.87)	3.63 (6.60)	96.35
PMP2/6-311G(2d,p)	13.77 (18.11)	14.02 (18.06)	2.67 (5.64)	
MP2/6-311G(3df,2p)	14.79 (19.14)	15.05 (19.09)	0.91 (3.88)	97.49
PMP2/6-311G(3df,2p)	11.97 (16.32)	12.21 (16.25)	−0.11 (2.86)	
MP2/6-311+G(3df,2p)	14.62 (18.96)	14.80 (18.84)	−0.68 (2.29)	97.53
PMP2/6-311+G(3df,2p)	11.86 (16.21)	12.04 (16.08)	−1.63 (1.33)	
QCISD(T)/6-311+G(3df,2p)	11.08 (15.43)	11.27 (15.31)	0.10 (3.06)	98.13
Expt.			0.51	98.9

[a] The values in parentheses are the values without ZPE correction. The experimental value of the C−H bond dissociation energy is obtained from ref 27. The values are in kcal/mol.

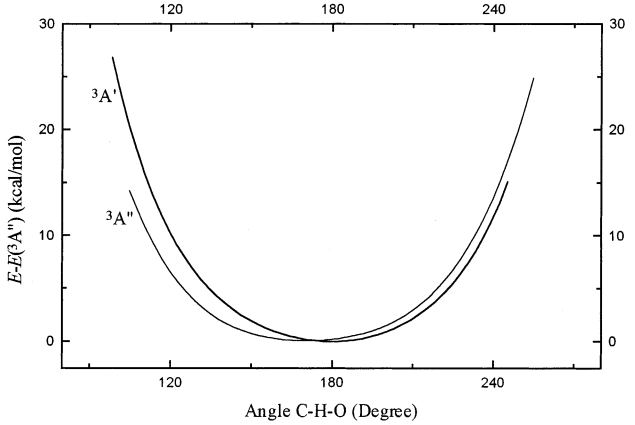

Figure 2. Energy profile for the ^{3}A′ and ^{3}A″ potential energy curves with respect to the C−H−O bending angle at the MP2/6-311G(2d,p) level. For these calculations, the other internal coordinates were fixed at their respective values in the minimum.

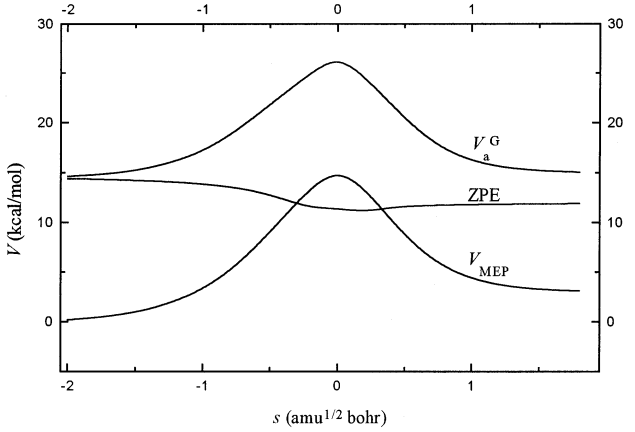

Figure 3. Potential energy (V_{MEP}) and vibrationally adiabatic potential energy (V_a^G) curves as functions of s at the QCISD(T)//MP2 level for the ^{3}A″ potential energy surface.

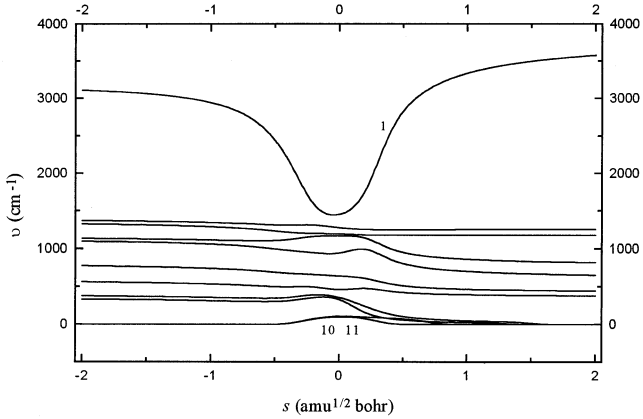

Figure 4. Changes of the generalized normal-mode vibrational frequencies as functions of s at the MP2/6-311G(2d,p) level for the ^{3}A″ potential energy surface.

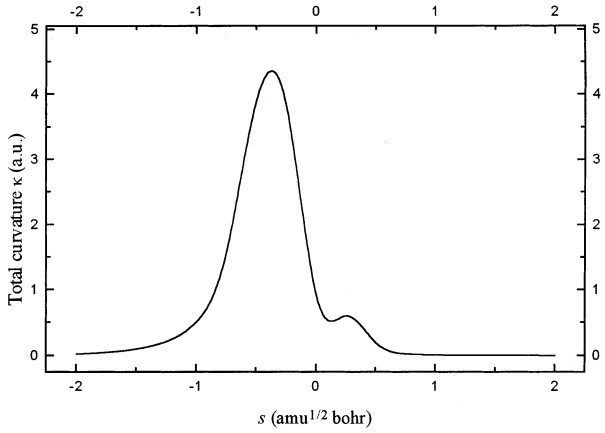

Figure 5. Total reaction path curvature as function of s at the MP2 level on the ^{3}A″ potential energy surface.

a pure triplet. Thus, spin contamination is not severe for the studied system. Figure 1 and Table 1 show the geometric parameters and frequencies of the equilibrium and saddle points at the MP2/6-311G(2d,p) level along with the available experimental data. It can be seen from Figure 1 that the geometric parameters of CHF_2Cl and OH optimized are in good agreement with the experimental values. From this result, it might be inferred that the same accuracy could be expected for the calculated saddle point geometries, but such an inference would be unjustified because saddle points are much harder to calculate. The vibrational frequencies of CHF_2Cl, CF_2Cl, and OH agree well with the experimentally observed fundamentals, and the maximum relative error is less than 6.0%. These good agreements give us confidence that the MP2/6-311G(2d,p) theory level is adequate to optimize the geometries and calculate the frequencies.

Next, we consider the saddle points, for which we performed a more detailed analysis. As mentioned above, the hydrogen abstraction reaction of O (^{3}P) with CHF_2Cl can proceed over two potential energy surfaces (PESs), ^{3}A′ + ^{3}A″, generated by the pseudo-Jahn−Teller effect. This kind of situation has been studied previously for the reaction of O (^{3}P) with CH_4,[28−29] where, because of the higher symmetry, it is a true Jahn−Teller effect. At the MP2/6-311G(2d,p) level, two saddle points with ^{3}A″ and ^{3}A′ symmetries were located, whose geometrical structures are shown in Figure 1. The saddle points of ^{3}A″ and ^{3}A′ symmetries are denoted as TS_1 and TS_2, respectively. For both ^{3}A″ and ^{3}A′ saddle points, the O (^{3}P) atom attacks the H

TABLE 3: Calculated TST, CVT, and CVT/SCT Rate Constants along with the Experimental Values[a]

T/K	TST	CVT	CVT/SCT	expt	
200	3.12×10^{-28}	2.97×10^{-28}	2.92×10^{-22}		
250	1.52×10^{-24}	1.45×10^{-24}	4.02×10^{-20}		
298	3.52×10^{-22}	3.35×10^{-22}	1.02×10^{-18}		
300	4.25×10^{-22}	4.05×10^{-22}	1.14×10^{-18}		9.67×10^{-18}[c]
350	2.33×10^{-20}	2.22×10^{-20}	1.28×10^{-17}		7.14×10^{-17}[c]
400	4.67×10^{-19}	4.45×10^{-19}	8.06×10^{-17}	2.83×10^{-16}[b]	3.20×10^{-16}[c]
450	4.78×10^{-18}	4.55×10^{-18}	3.44×10^{-16}	9.15×10^{-16}[b]	1.03×10^{-15}[c]
500	3.08×10^{-17}	2.93×10^{-17}	1.12×10^{-15}	2.34×10^{-15}[b]	2.61×10^{-15}[c]
550	1.41×10^{-16}	1.34×10^{-16}	2.99×10^{-15}	5.05×10^{-15}[b]	5.61×10^{-15}[c]
600	5.02×10^{-16}	4.78×10^{-16}	6.90×10^{-15}	9.58×10^{-15}[b]	1.06×10^{-14}[c]
620	7.89×10^{-16}	7.52×10^{-16}	9.31×10^{-15}	1.20×10^{-14}[b]	
700	3.73×10^{-15}	3.55×10^{-15}	2.66×10^{-14}	2.88×10^{-14}[c]	
800	1.71×10^{-14}	1.63×10^{-14}	7.69×10^{-14}	6.10×10^{-14}[c]	
900	5.64×10^{-14}	5.37×10^{-14}	1.82×10^{-13}	1.09×10^{-13}[c]	
1000	1.48×10^{-13}	1.41×10^{-13}	3.72×10^{-13}	1.74×10^{-13}[c]	
1200	6.55×10^{-13}	6.23×10^{-13}	1.16×10^{-12}		
1400	1.96×10^{-12}	1.87×10^{-12}	2.80×10^{-12}		
1600	4.57×10^{-12}	4.35×10^{-12}	5.66×10^{-12}		
1800	9.01×10^{-12}	8.58×10^{-12}	1.01×10^{-11}		
2000	1.58×10^{-11}	1.51×10^{-11}	1.65×10^{-11}		
2200	2.54×10^{-11}	2.42×10^{-11}	2.51×10^{-11}		
2400	3.82×10^{-11}	3.63×10^{-11}	3.62×10^{-11}		
2600	5.43×10^{-11}	5.17×10^{-11}	5.00×10^{-11}		
2800	7.42×10^{-11}	7.07×10^{-11}	6.67×10^{-11}		
3000	9.78×10^{-11}	9.32×10^{-11}	8.62×10^{-11}		

[a] The values are in cm^3 $molecule^{-1}$ s^{-1}. [b] The values are obtained from ref 14. [c] The values are obtained from ref 15.

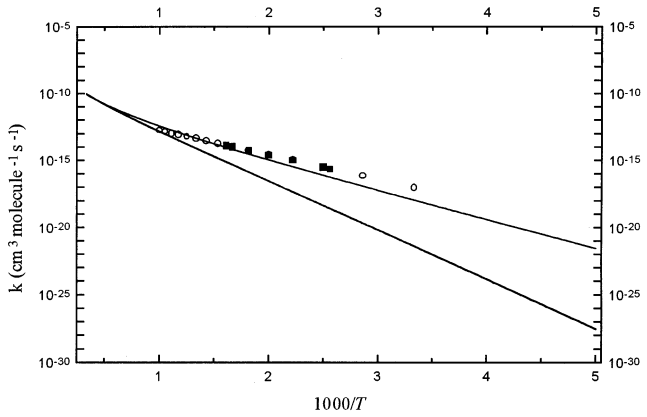

Figure 6. Arrhenius plot of the rate constants in the temperature range of 200∼3000 K for the whole reaction of O (^{3}P) with CHF_2Cl. ■ and ○ are the experimental values.[14−15]

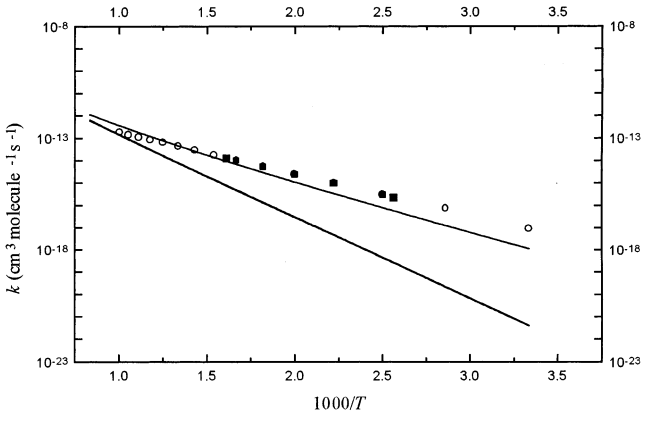

Figure 7. Arrhenius plot of the rate constants in the temperature range of 350∼1000 K for the whole reaction of O (^{3}P) with CHF_2Cl. ■ and ○ are the experimental values.[14−15]

atom of CHF_2Cl from the trans position of the Cl atom. Population analysis shows that the half-filled p orbital of the ^{3}A″ symmetry is in ClCHO plane and the half-filled p orbital of the ^{3}A′ symmetry is perpendicular to this plane. The ^{3}A″ and ^{3}A′ saddle points were almost identical in energy but differ slightly in the C−H−O bending angle. The C−H−O angle is 170.2° for the saddle point with ^{3}A″ symmetry, whereas this angle is 179.8° for the one with ^{3}A′ symmetry. Therefore, the ^{3}A″ saddle point is more "bent" than the ^{3}A′ one. The breaking C−H bonds are elongated by 16.7% and 16.7%, whereas the forming O−H bonds are longer than the equilibrium value of 0.970 Å by 23.3% and 23.1% for the saddle points of ^{3}A″ and ^{3}A′ symmetries. Therefore, these two saddle points are reactant-like.

The saddle points were identified with one negative eigenvalue of the respective Hessian matrix and, therefore, one imaginary frequency. Because the imaginary frequency governs the width of the classical potential energy barrier along the MEP, it plays an important role in the tunneling calculations, especially when the imaginary frequency is large, and the associated eigenvector has a large component of hydrogenic motion. For the title reaction, the imaginary frequencies are 2663i and 2674i for ^{3}A″ and ^{3}A′ saddle points, so we expect that the tunneling effect should be important for the calculation of the rate constant. It also can be seen from Table 2 that the saddle points TS_1 and TS_2 have very similar vibrational frequencies, in accordance with their very similar geometrical parameters and energies.

To get a clearer view of the ^{3}A″ and ^{3}A′ surfaces, we have carried out electron structure calculations at the MP2/6-311G-(2d,p) level, varying the angle C−H−O in relation to its respective optimized saddle point geometry. Figure 2 shows the calculations of the PESs in C_s symmetry, where energies are referred to the most stable ^{3}A″ structure and the internuclear distances, *d*(C−H) and *d*(H−O), are fixed. The calculated PES is very flat, and in the region of 170−180°, the difference in energy between the ^{3}A″ and ^{3}A′ electronic PES is less than 0.1 kcal/mol.

To further confirm that these two saddle points of ^{3}A″ and ^{3}A′ symmetries connect the designated reactants and products, the intrinsic reaction coordinate (IRC) has been calculated at the MP2/6-311G(2d,p) level from the saddle point to the reactants and the products. For these two saddle points of ^{3}A″ and ^{3}A′ symmetries, the profiles of the changing of the bond

lengths along the reaction path are almost overlapping. The breaking C−H bond is almost unchanged from $s = -\infty$ to $s = -0.5$ amu$^{1/2}$ bohr and equals the value in the reactant, and stretches after $s = -0.5$ amu$^{-1/2}$ bohr. The forming H−O bond shortens rapidly from reactants and reaches the equilibrium bond length in OH at $s = 0.7$ amu$^{1/2}$ bohr. Other bond lengths are almost unchanged during the reaction process. Therefore, the saddle points of ^{3}A″ and ^{3}A′ symmetries both connect the reactants (CHF_2Cl and O) with the products (CF_2Cl and OH). The geometric change mainly takes place in the region from $s = -0.5$ to $s = 0.7$ amu$^{1/2}$ bohr. This means that the region of the hydrogen abstraction reaction path represents the main interaction of the reaction process.

b. Energy. To choose a reliable theory level to calculate the energy, the C−H bond dissociation energy was calculated for the CHF_2Cl. The obtained values at various levels along with the experimental value are depicted in Table 2. The experiment gave the spectroscopic dissociation energy, and so the calculated dissociation energies were corrected for the ZPE. It can be seen that the MP2 level with 6-311G(2d,p) and 6-311+G(3df,2p) basis sets underestimates the bond dissociation energy. The calculated result at the QCISD(T)/6-311+G(3df,2p) level is in good agreement with the experimental value. Therefore, the QCISD(T)/6-311+G(3df,2p) level is a good choice to calculate accurate energies for the title system.

First, we analyze the reaction enthalpy. We obtained an experimental value of 0.51 kcal/mol from the experimental standard heats of formation $\Delta H_{f,0}$ for O, CHF_2Cl, and OH[26,30] together with the calculated $\Delta H_{f,0}$ for CF_2Cl. The values of 3.63 and −0.68 kcal/mol calculated at the MP2/6-311G(2d,p) and MP2/6-311+G(3df,2p) levels are in great disagreement with the experimental value, and similar calculation with the highly correlated and more computationally demanding QCISD(T)/6-311+G(3df,2p) level predict the value of 0.10 kcal/mol, in excellent agreement with the experimental value. This results clearly indicated that most of the error in the reaction enthalpy computed at the MP2 level can be attributed to the lack of correlation in such a method and not to an improper optimized geometry at the MP2/6-311G(2d,p) level.

With respect to the potential barrier, the values are almost identical for the two potential energy surfaces of ^{3}A″ and ^{3}A′ symmetries at the same level. It means the two saddle points are almost degenerate in energy. However, the values for the same potential energy surface have a great discrepancy obtained at the MP2 and QCISD(T) levels. It is well-known that the potential barrier may be overestimated at the MP2 level because of the spin contamination.[31] The barrier height obtained from the PMP2 energies is thus considered to be more reliable. In the present case, the potential barriers obtained from the MP2 energies are found to be more than 2.5 kcal/mol higher than these obtained from the corresponding PMP2 energies with the same basis set. The effect of basis set on the potential barrier can be observed from our MP2 result with three different basis sets, namely, 6-311G(2d,p), 6-311G(3df,2p), and 6-311+G(3df,2p). The barrier heights decrease by about 2 kcal/mol with the increase in polarization function (6-311G(2d,p) → 6-311G(3df,2p)) at the MP2 level for the surfaces of ^{3}A″ and ^{3}A′ symmetries, whereas the barrier heights decrease by only 0.2 kcal/mol with the increase in diffuse function (6-311G(3df,2p)→6-311+G(3df,2p)). As we raise the calculation levels (MP2→QCISD(T), with the same basis set), the barrier height is lowered drastically. Taking into account the calculated results of the C−H bond dissociation energy at these levels, we think the QCISD(T)/6-311+G(3df,2p) level is the most reliable level. Therefore, in this paper, we choose the energies calculated at the QCISD(T)/6-311+G(3df,2p) level for the following kinetics calculation.

3.2. Kinetics Calculation. The reaction kinetics on the ^{3}A″ and ^{3}A′ surfaces has been calculated independently. The two surfaces show similar features, and further discussion in this paper will refer only to the ^{3}A″ surface.

a. Reaction Path Properties. The minimum energy path (MEP) was calculated at the MP2/6-311G(2d,p) level by the IRC definition, and the energies of the MEP were refined by the QCISD(T) //MP2 method. For this reaction, the maximum position of the classical potential energy curve V_{MEP} at the QCISD(T) //MP2 level corresponds to the saddle point structure at the MP2/6-311G(2d,p) level. Therefore, the shifting of the maximum position for the V_{MEP} curve caused by the computational technique is avoided (avoiding artificial variational effect).[32−33] The changes of the classical potential energy V_{MEP} and the ground-state vibrational adiabatic potential energy V_a^G with the reaction coordinate s on the ^{3}A″ potential surface are shown in Figure 3. The V_{MEP} and V_a^G curves are similar in shape, and their maximum positions are almost the same at the QCISD(T)//MP2 level. It means that the variational effect will be small for this reaction. The zero-point energy ZPE, which is the difference of V_a^G and V_{MEP}, is also shown in Figure 3. The zero-point energy curve is almost unchanged as s varies except that only from $s = -1.0$ to 1.0 amu$^{1/2}$ bohr there is a gentle valley. To analyze this behavior in greater detail, we show the variation of the generalized normal modes vibrational frequencies on the ^{3}A″ potential surface in Figure 4.

In the negative limit of s, the frequencies are associated with the reactants (CHF_2Cl+O), whereas in the positive limit of s, the frequencies are associated with the products (CF_2Cl+OH). The vibrational mode 1 (reactive mode) that connects the frequency of C−H stretching vibration in CHF_2Cl with the frequency of the O−H stretching vibration of OH drops dramatically from $s = -1.0$ to 1.0 amu$^{1/2}$ bohr, and this behavior is similar to that found in other hydrogen abstraction reactions.[34,35] If changes in other frequencies were small, this drop could cause a considerable fall in the zero-point energy near the saddle point. The two lowest harmonic vibrational frequencies (modes 10 and 11, transitional modes) along the reaction path correspond to the transformation of free rotations or free translations of the reactant limit into real vibrational motions in the global system. Their frequencies tend asymptotically to zero at the reactant and product limits and reach their maximum in the saddle point zone. Therefore, in the saddle point region, the behavior of these transitional modes partially compensates the fall in the zero-point energy caused by the mode 1. As a result, the zero-point energy curve shows a gentle drop in the saddle point zone.

Further analyzing the reaction valley, the curvature term (κ) of the reaction path as function of s is plotted in Figure 5. There are two sharp peaks, one before and one after the saddle point. The positions of the peaks are at $s = -0.37$ and 0.26 amu$^{1/2}$ bohr, because of the strong coupling of the reaction coordinate with the C−H and O−H stretches, respectively. The second peak is lower than the first. Notice that the reaction path curvature of this reaction is not severe; therefore, the small-curvature tunneling correction method for calculating the reaction rate constants should be suitable.

b. Rate Constant. The canonical variational transition state theory (CVT) with a small-curvature tunneling correction (SCT), which has been successfully performed for several analogous reactions,[36−38] is an efficient method to calculate the rate

constant. In this paper, we used this method to calculate the rate constants for the reaction of the O atom with CHF_2Cl over a wide temperature range from 200 to 3000 K.

To calculate the rate constant, 30 points were selected near the saddle point along the MEP, 15 points in the reactant zone, and 15 points in the product zone. Table 3 and Figure 6 shows the total rate constant, which is obtained as the sum of the calculated CVT/SCT rate constants for the $^3A''$ and $^3A'$ surfaces, and the experimental values against the reciprocal of the temperature for the reaction of O (^3P) with CHF_2Cl over the temperature range of 200∼3000 K. For the purpose of comparison, the conventional transition state theory (TST) rate constants and the variational transition state theory (CVT) rate constants without the tunneling correction are also shown in Table 3 and Figure 6. Several important features of the calculated rate constants are the following:

(1) It can be seen that the rate constants of TST and CVT are nearly the same in the whole studied temperature range of 200∼3000 K, which enables us to conclude that the variational effect is small for the calculation of the rate constant. It is in accordance with the above analysis.

(2) Reactions involving hydrogen atom transfer are usually characterized significant tunneling effect that must be accounted for when computing reaction rate constants. In the present case, the CVT/SCT rate constants are greater than the CVT ones over the temperature range of 200∼1500 K. For example, at 298 K, the CVT rate constant is 3.35×10^{-22} cm^3 molecule^{-1} s^{-1}, whereas the CVT/SCT rate constant is 1.01×10^{-18} cm^3 molecule^{-1} s^{-1}. The latter is 4328 times larger than the former. At 1000 K, the CVT rate constant is 1.41×10^{-13} cm^3 molecule^{-1} s^{-1}, whereas the CVT/SCT rate constant is 3.72×10^{-13} cm^3 molecule^{-1} s^{-1}. The latter is 2.64 times larger than the former. The difference between the CVT rate constant and the CVT/SCT rate constant decreases with the increase in temperature. When the temperature is higher than 1500 K, the CVT/SCT rate constants are asymptotic to the rate constants of CVT, which means only in the lower temperature range the small-curvature tunneling correction plays an important role for the calculation of the rate constant. The contribution of tunneling becomes progressively less important as the temperature rises. To compare, we calculated the rate constants with zero-curvature tunneling (ZCT) correction. The CVT/SCT rate constants are greater than the CVT/ZCT ones over the temperature range of 200∼550 K. For example, at 200 K, the CVT/SCT rate constant is 2.92×10^{-22} cm^3 molecule^{-1} s^{-1}, whereas the CVT/ZCT rate constant is 2.12×10^{-25} cm^3 molecule^{-1} s^{-1}. The former is 1372 times larger than the latter. When the temperature is higher than 550 K, the CVT/ZCT rate constants are asymptotic to the rate constants of CVT/SCT. For example, at 600 K, the CVT/SCT rate constant is 6.90×10^{-15} cm^3 molecule^{-1} s^{-1}, whereas the CVT/ZCT rate constant is 5.46×10^{-15} cm^3 molecule^{-1} s^{-1}.

(3) To obtain a clearer comparison of the calculated rate constants with the experimental values for the title reaction, we plotted TST rate constants, CVT rate constants, and CVT/SCT rate constants along with the experimental values over the temperature range of 350∼1000 K in Figure 7. In the temperature range of 500∼620 K, the CVT/SCT rate constants deviate from the corresponding experimental values by no more than a factor of 2, and the CVT/SCT rate constants are in much better agreement with the experimental values. In the temperature range of 390∼500 K, the calculated CVT/SCT rate constants are slightly smaller than the values obtained from the experimental Arrhenius expression fitted by Gourdain. For example, at 400 K, the CVT/SCT rate constant is 8.06×10^{-17} cm^3 molecule^{-1} s^{-1}, weheras the experimental value is 2.83×10^{-16} cm^3 molecule^{-1} s^{-1}. The experimental value is about a factor of 3.5 larger than the theoretical rate constant. Certainly, those earlier experimental results may not be conclusive because in this temperature range the rate constant is so small that it is very difficult to obtain an accurate experimental value. The observed discrepancy between the theoretical rate constants and the experimental values at low temperature could also be due to an underestimate of the tunneling factor, and it is possible that a more sophisticated method for its estimate than that of the SCT method could reduce the differences. For example, for the similar $CH_4 + O$ reaction,[28] rate constants calculated using the SCT method and an optimized multidimensional method for tunneling differ by a factor of 18 at 300 K, the later being closer to the experimental values than the former.

(4) It is obvious that the calculated rate constants exhibit typical non-Arrhenius behavior. The rate constants of the title reaction are fitted by three-parameter formulas over the temperature range of 200∼3000 K and given in units of cm^3 molecule^{-1} s^{-1} as follows:

$$k(T) = 2.61 \times 10^{-12} T^{0.77} \exp(-8112.34/T), \quad \text{for TST rate constants}$$

$$k(T) = 2.49 \times 10^{-12} T^{0.77} \exp(-8112.35/T), \quad \text{for CVT rate constants}$$

$$k(T) = 4.75 \times 10^{-18} T^{2.26} \exp(-4318.02/T), \quad \text{for CVT/SCT rate constants}$$

(5) The rate constants are almost the same for the $^3A''$ and $^3A'$ surfaces, because of the nearly degenerate barrier height. For example, at 298 K, the CVT/SCT rate constant of the $^3A''$ surface is 5.36×10^{-19} cm^3 molecule^{-1} s^{-1}, whereas the value is 4.85×10^{-19} cm^3 molecule^{-1} s^{-1} for the $^3A'$ surfaces. At 1000 K, the CVT/SCT rate constant of the $^3A''$ surface is 1.92×10^{-13} cm^3 molecule^{-1} s^{-1}, whereas the value is 1.80×10^{-13} cm^3 molecule^{-1} s^{-1} for the $^3A'$ surfaces.

(6) At low temperature, the rate constants for the reaction of O (^3P) with CHF_2Cl are relatively small. Therefore, this reaction cannot occur to any significant extent under the atmospheric condition. However, the rate constants increase rapidly with elevation of temperature. At 3000 K, the rate constant of the reaction is 8.62×10^{-11} cm^3 molecule^{-1} s^{-1}. So the reaction should play an important role under high-temperature combustion conditions.

4. Conclusion

In this paper, we studied the reaction of O (^3P) with CHF_2Cl using ab initio and canonical variational transition state theory (CVT) with small-curvature tunneling effect. Rate constants were reported over the temperature range of 200∼3000 K. Several major conclusions can be drawn from this calculation.

1. This reaction proceeds via a direct hydrogen abstraction mechanism.

2. For this hydrogen abstraction reaction, the approach of the O (^3P) to CHF_2Cl with C_s symmetry proceeds over two potential energy surfaces (PESs), $^3A' + {}^3A''$, generated by the pseudo-Jahn−Teller effect.

3. The calculated rate constants exhibit typical non-Arrhenius behavior.

4. In the temperature range of 500∼620 K, the calculated CVT/SCT rate constants are in good agreement with the

experimental values. In the temperature range of 390∼500 K, the calculated rate constants are slightly smaller than the experimental values.

Acknowledgment. The authors thank Professor Donald G. Truhlar for providing the POLYRATE 7.8 program. This work is supported by the Research Fund for the Doctoral Program of Higher Education of China.

References and Notes

(1) Tuck, R.; Plumb, A.; Condon, E. *Geophys. Res. Lett*. **1990**, *17*, 313.

(2) Manzer, L. *Science* **1990**, *249*, 31.

(3) Atkinson, R. *Chem. Rev*. **1986**, *86*, 69.

(4) Baes, G. *ANPI Mag*. **1992**, *112*, 43.

(5) Banks, R. E. *J. Fluorine Chem*. **1994**, *67*, 193.

(6) Smith, K. M.; Duxburg, G.; Newnham, D. A.; Ballard, J. *J. Chem. Soc., Faraday Trans*. **1997**, *93*, 2735.

(7) Miziolek, A. W.; Tsang, W. *Halon Replacements: Technology and Science*; ACS Symp. Ser. 611; American Chemical Society: Washington, DC, 1995.

(8) Tuazon, E. C.; Atkinson, R.; Corchnoy, S. B. *Int. J. Chem. Kinet*. **1992**, *24*, 639.

(9) Talhaoui, A.; Louis, F.; Meriaux, B.; Devolder, P.; Sawerysyn, J. P. *J. Phys. Chem*. **1996**, *100*, 2107.

(10) Jeong, K. M.; Kaufman, F. *J. Phys. Chem*. **1982**, *86*, 1808.

(11) Berry, R. J.; Ehlers, C. J.; Burgess, D. R., Jr.; Zachariah, M. R.; Marshall, P. *Chem. Phys. Lett*. **1997**, *269*, 107.

(12) Medhurst, L. J.; Fleming, J.; Nelson, H. H. *Chem. Phys. Lett*. **1997**, *266*, 607.

(13) Laurent, T.; Lillich, H.; Volpp, H. R.; Wolfrum, J.; Bar, I.; Melchior, A.; Rosenwaks, S. *Chem. Phys. Lett*. **1995**, *247*, 321.

(14) Jourdain, J. L.; Poulet, G.; Barassin, J.; LeBras, G.; Combourieu, J. *Pollut. Atmos.* **1977**, *75*, 256.

(15) Herron, J. T. *J. Phys. Chem. Ref. Data* **1988**, *17*, 967.

(16) Baldrige, K. K.; Gordon, M. S.; Steckler, R.; Truhlar, D. G. *J. Phys. Chem*. **1989**, *93*, 5107.

(17) Gonzalez-Lafont, A.; Truong, T. N.; Truhlar, D. G. *J. Chem. Phys*. **1991**, *95*, 8875.

(18) Garrett, B. C.; Truhlar, D. G. *J. Phys. Chem.* **1979**, *83*, 1052.

(19) Liu, Y.-P.; Lynch, G. C.; Truong, T. N.; Lu, D.-H.; Truhlar, D. G.; Garrett, B. C. *J. Am. Chem. Soc.* **1993**, *115*, 2408.

(20) Frisch, M. J.; Trucks, G. W.; Schlegel, H. B.; Gill, P. M. W.; Johnson, B. G.; Robb, M. A.; Cheeseman, J. R.; Keith, T.; Petersson, G. A.; Montgomery, J. A.; Raghavachari, K.; Al-Laham, M. A.; Zakrzewski, V. G.; Ortiz, J. V.; Foresman, J. B.; Cioslowski, J.; Stefanov, B. B.; Nanayakkara, A.; Challacombe, M.; Peng, C. Y.; Ayala, P. Y.; Chen, W.; Wong, M. W.; Andres, J. L.; Replogle, E. S.; Gomperts, R.; Martin, R. L.; Fox, D. J.; Binkley, J. S.; Defrees, D. J.; Baker, J.; Stewart, J. P.; Head-Gordon, M.; Gonzalez, C.; Pople, J. A. *Gaussian 94*, revision E.1; Gaussian, Inc.: Pittsburgh, PA, 1995.

(21) Frisch, M. J.; Head-Gordon, M.; Pople, J. A. *Chem. Phys. Lett.* **1990**, *166*, 281.

(22) Pople, J. A.; Head-Gordon, M.; Raghavachari, K. J. *Chem. Phys.* **1987**, *87*, 5968.

(23) Steckler, R.; Chuang, Y. Y.; Fast, P. L.; Corchado, J. C.; Coitino, E. L.; Hu, W. P.; Lynch, G. C.; Nguyen, K.; Jackels, C. F.; Gu, M. Z.; Rossi, I.; Clayton, S.; Melissas, V.; Garrett, B. C.; Isaacson, A. D.; Truhlar, D. G. *POLYRATE Version*; University of Minnesota, Minneapolis, MN, 1997.

(24) Truong, T. N.; Lu, D.-H.; Lynch, G. C.; Liu, Y. P.; Melissas, V. S.; Stewart, J. J. P.; Steckler, R.; Garrett, B. C.; Isaacson, A. D.; Gonzalez-Lafont, A.; Rai, S. N.; Hancock, G. C.; Joseph, T.; Truhlar, D. G. *Comput. Phys. Commun*. **1993**, *75*, 43.

(25) Harmony, M. P.; Laurie, V. W.; Ramsay, R. L.; Lovas, F. J.; Lafferty, W. J.; et al. *J. Phys. Chem. Ref. Data* **1979**, *8*, 619.

(26) Chen, S. S.; Wilhoit, R. C.; Zwolinski, B. J. *J. Phys. Chem. Ref. Data* **1976**, *5*, 571.

(27) *CRC Handbook of Chemistry and Physics*, 78th ed.; Lide, D. R., Ed.; CRC Press: Boca Raton, FL, 1997.

(28) Corchado, J. C.; Espinosa-Garcia, J.; Roberto-Neto, O.; Chuang, Y.-Y.; Truhlar, D. G. *J. Phys. Chem. A* **1998**, *102*, 4899.

(29) Gonzalez, M.; Hernando, J.; Millan, J.; Sayos, R. *J. Chem. Phys*. **1999**, *110*, 7326.

(30) Chase, M. W., Jr.; Davies, C. A.; Downey, J. R., Jr.; Frurip, D. J.; McDonald, R. A.; Syverud, A. N. JANAF Thermochemical Table. *J. Phys. Chem., Ref. Data* **1985**, 14 Suppl. No. 1.

(31) Gonzalez, C.; Sosa, C.; Schlegel, H. B. *J. Phys. Chem*. **1989**, *93*, 2435.

(32) Malick, D. K.; Petersson, G. A.; Montgomery, J. A., Jr. *J. Chem. Phys*. **1998**, *108*, 5704.

(33) Espinosa-Garcia, J.; Corchado, J. C. *J. Phys. Chem*. **1995**, *99*, 8613.

(34) Truhlar, D. G.; Isaacson, A. D. *J. Chem. Phys*. **1982**, *77*, 3516.

(35) Corchado, J. C.; Espinosa-Garcia, J. *J. Chem. Phys*. **1997**, *106*, 4013.

(36) Espinosa-Garcia, J. *J. Phys. Chem. A* **2000**, *104*, 7537.

(37) Melissas, V. S.; Truhlar, D. G. *J. Phys. Chem*. **1994**, *98*, 875.

(38) Melissas, V. S.; Truhlar, D. G. *J. Chem. Phys*. **1993**, *99*, 1013.